

Class II PI3Ks α and β Are Required for Rho-Dependent Uterine Smooth Muscle Contraction and Parturition in Mice

メタデータ	言語: eng 出版者: 公開日: 2019-04-25 キーワード (Ja): キーワード (En): 作成者: メールアドレス: 所属:
URL	https://doi.org/10.24517/00053884

This work is licensed under a Creative Commons Attribution-NonCommercial-ShareAlike 3.0 International License.



1 **Class II PI3K α and β are required for Rho-dependent uterine smooth muscle**
2 **contraction and parturition in mice**

3

4 Md Azadul Kabir Sarker, Sho Aki, Kazuaki Yoshioka, Kouji Kuno, Yasuo Okamoto,
5 Kazuhiro Ishimaru, Noriko Takuwa, Yoh Takuwa

6

7 Department of Physiology (M.A.K.S., S.A., K.Y., Y.O., K.I., Y.T.), Kanazawa

8 University School of Medicine, Kanazawa 920-8640, Japan; Cancer Research Institute

9 (K.K.), Kanazawa University, Kanazawa 920-0934, Japan; Department of Health

10 Science (N.T.), Ishikawa Prefectural University, Kahoku 929-1210, Japan

11

12 **Short title:** Class II PI3K requirement for uterine contraction

13

14 **Keywords:** class II PI3K, PI3K-C2 α , PI3K-C2 β , uterus, smooth muscle contraction,
15 parturition

16

17 **Corresponding author:** Yoh Takuwa, M.D., Ph.D.

18 ytakuwa@med.kanazawa-u.ac.jp, TEL +81-76-265-2165, FAX +81-76-265-4223

19

20 **Reprint requests should be addressed to:** Yoh Takuwa, M.D., Ph.D., Department of
21 Physiology, 13-1 Takara-machi, Kanazawa University School of Medicine, Kanazawa,
22 Ishikawa 920-8640, Japan

23

24 **Sources of Funding:** This study was supported by grants from the Ministry of
25 Education, Culture, Sports, Science and Technology (MEXT) of Japan (25116711 to
26 Y.T.), and the Japan Society for the Promotion of Science (17K08532 to K.Y.,
27 16K18988 to S.A., 17K08542 to N.T., 15H04673 to Y.T.).

28

29 **Disclosure:** All authors declare that they have no conflict of interest.

30

31

32

33

34

35

36

37 **Abstract**

38 Class II phosphoinositide 3-kinases (PI3K), PI3K-C2 α and PI3K-C2 β , are highly
39 homologous and distinct from class I and III PI3K in the catalytic products and domain
40 structures. In contrast to class I and class III PI3Ks, physiological roles of PI3K-C2 α
41 and PI3K-C2 β are not fully understood. Because we previously demonstrated that
42 PI3K-C2 α is involved in vascular smooth muscle contraction, we studied the
43 phenotypes of smooth muscle-specific knockout (KO) mice of PI3K-C2 α and
44 PI3K-C2 β . The pup numbers born from single PI3K-C2 α -KO and single PI3K-C2 β -KO
45 mothers were similar to those of control mothers, but that from double KO (DKO)
46 mother was smaller compared with control mice. However, the number of intrauterine
47 fetuses in pregnant DKO mothers was similar to that in control mice. Both spontaneous
48 and oxytocin-induced contraction of isolated uterine smooth muscle (USM) strips was
49 diminished in DKO mice but not either of the single KO mice, compared with control
50 mice. Furthermore, contraction of USM of DKO mice was less sensitive to a Rho kinase
51 inhibitor. Mechanistically, the extent of oxytocin-induced myosin light chain
52 phosphorylation was greatly reduced in USM from DKO mice compared with control
53 mice. Oxytocin-induced rise in the intracellular Ca²⁺ concentration in USM was similar
54 in DKO and control mice. However, Rho activation in the intracellular compartment

55 was substantially attenuated in DKO mice compared with control mice, as evaluated by
56 fluorescence resonance energy transfer imaging technique. These data indicate that both
57 PI3K-C2 α and PI3K-C2 β are required for normal USM contraction and parturition
58 mainly through their involvement in Rho activation.

59

60

61

62

63

64

65

66

67

68

69

70

71

72

73 **Introduction**

74 Reproduction is highly coordinated by various hormones and local mediators with
75 the integration by the neuroendocrine system (1,2). The uterus, one of the most
76 important female reproductive organs, accommodates and nurtures the growing fetus (3).
77 The uterus comprises three layers: the endometrial, myometrial and outer serosal layers.
78 During the pregnancy, the myometrium remains quiescent and undergoes enormous
79 hyperplasia and hypertrophy to provide proper environment for fetal growth and to
80 prepare for the generation of uterine contractile force sufficient for fetal delivery. At the
81 last stage of pregnancy, stretching of the uterine wall by the grown-up fetus and other
82 changes in the local uterine environment causes the activation of the myometrium,
83 bringing about myometrial alterations including the extreme upregulation of oxytocin
84 receptor and voltage-dependent Ca^{2+} channel (4,5).

85 Phosphoinositide 3-kinases (PI3Ks) are lipid kinases that catalyze the
86 phosphorylation at 3'-hydroxyl group of the inositol ring in phosphoinositides (6).
87 PI3Ks comprise three classes of PI3Ks; class I PI3Ks, p110 α , p110 β , p110 γ and p110 δ ,
88 are activated downstream of various receptor tyrosine kinases and G protein-coupled
89 receptors, to mainly generate phosphatidylinositol 3,4,5-trisphosphate (PI(3,4,5)P₃) and
90 to mediate cell proliferation, survival and migration. Class III PI3K, Vps34, mainly

91 regulates autophagy by generating phosphatidylinositol 3-phosphate (PI(3)P). Class II
92 PI3Ks comprise PI3K-C2 α (C2 α), PI3K-C2 β (C2 β), and PI3K-C2 γ (C2 γ), which
93 generate phosphatidylinositol 3,4-bisphosphate (PI(3,4)P₂) and probably PI(3)P (7-9).
94 C2 α and C2 β are ubiquitously expressed widely in various organs and tissues whereas
95 C2 γ expression is restricted mainly in liver, breast, testis and prostate (10). In contrast to
96 class I and class III PI3Ks, the physiological function of class II PI3Ks was not well
97 understood.

98 We previously demonstrated using siRNA-mediated specific knockdown technique
99 that C2 α was required for noradrenaline- and ionomycin-induced contraction of
100 vascular smooth muscle cells (11-13). Subsequently, we generated C2 α -knockout (KO)
101 mice to study a role of C2 α at an organismal level and found that homozygous C2 α -KO
102 mice were embryonic lethal due to severe vascular endothelial defects (14).
103 C2 α -deficient vascular endothelial cells showed impairment of Rho activation in the
104 endosomes in response to the angiogenic factor VEGF due to defects of VEGF receptor
105 internalization, which led to impaired proliferation, migration and cell-cell adhesion of
106 endothelial cells (14). Furthermore, we observed in endothelial cells that endosomal
107 activation of Rac and Smad2/3 was also impaired upon stimulation by
108 sphingosine-1-phosphate (S1P) and TGF β 1, respectively, due to defects in the

109 internalization of S1P receptor and TGF β 1 receptor (9,15). These findings suggested
110 that C2 α is required for receptor endocytosis and subsequent receptor signaling in the
111 endosomes for at least certain receptor ligands in endothelial cells. C2 β is highly
112 homologous in its amino acid sequence to C2 α and exhibits similar activities including
113 cell migration and growth compared with C2 α . However, it is little known how
114 important C2 β is in endocytosis and the intracellular signaling (16).

115 In the present study, we sought to reveal physiological roles of C2 α and C2 β in
116 smooth muscle organs by generating smooth muscle-specific KO mice of C2 α and C2 β .
117 During this study, we found that pregnant smooth muscle-specific double KO (smDKO)
118 female mice, but not single KO mice of either C2 α or C2 β , delivered smaller numbers
119 of pups compared with control mice although the numbers of fetuses in the uteri at the
120 term pregnancy did not differ between smDKO and control mice. Isolated uterine
121 smooth muscle from smDKO mice showed attenuated contraction with reduced
122 intracellular Rho activation, compared with control mice. These results indicate the
123 novel physiological role of C2 α and C2 β in uterine smooth muscle contraction and pup
124 delivery.

125

126

127 **Materials and Methods**

128 **Materials**

129 Advanced DMEM (Gibco, cat no. 12491-015) and FluoroBrite DMEM (Gibco, cat
130 no. A1896701) were purchased from Gibco/Life Technologies Corporation, NY. Fluo-8
131 AM (cat no. 21081) was purchased from AAT Bioquest, Sunnyvale, CA. Liberase TM
132 (cat no. 5401127001) and protease inhibitor cocktail Complete mini (Cat. no.
133 11836153001) were purchased from Roche, Mannheim, Germany. Y-27632 (Cat no.
134 253-00513) and normal goat serum (cat no. 143-06561) were purchased from Wako
135 Pure Chemicals Industries, Osaka, Japan. Oxytocin (cat no. O6379), nitrendipine (cat no.
136 N144) and other chemicals were bought from Sigma-Aldrich, Saint Louis, MO unless
137 others specified. The following antibodies were used in this study: rabbit polyclonal
138 PI3K-C2 α (cat no. AP1155B, Abgent, San Diego, CA), rabbit polyclonal PI3K-C2 β
139 (cat no. sc-134766, Santa Cruz, Dallas, TX), rabbit polyclonal anti-smooth muscle
140 myosin heavy chain 11 (cat no. ab53219, Abcam, Cambridge, UK), mouse monoclonal
141 anti-caldesmon (cat no. C-6542, Sigma-Aldrich, Saint Louis, MO), monoclonal
142 anti-myosin light chain kinase (MLCK) (cat no. M 7905, Sigma-Aldrich, Saint Louis,
143 MO), rabbit polyclonal PP1 δ antibody (17), mouse monoclonal anti-calponin (cat no.
144 C2687, Sigma-Aldrich, Saint Louis, MO), rabbit polyclonal phospho-myosin

145 phosphatase target subunit-1 (MYPT1) (Thr⁸⁵³) (cat no.4563, Cell Signaling
146 Technologies, Danvers, MA), mouse monoclonal anti-MYPT1 (cat no. 612165, BD
147 Biosciences San Jose, CA), rabbit monoclonal PI3 Kinase Class II α (D3Q5B) from Cell
148 Signaling Technologies, Danvers, MA (Ref#12402), mouse monoclonal anti-PI3K-C2 β
149 antibody from BD Biosciences, San Jose, CA (Material number 611342), rabbit
150 polyclonal phospho-MLC₂₀ (Ser¹⁹) (cat no. 3671, Cell Signaling Technologies, Danvers,
151 MA), mouse monoclonal anti-myosin light chain (product no. M4401, Sigma-Aldrich,
152 Saint Louis, MO), mouse monoclonal anti-actin, α -smooth muscle (cat no. A5228,
153 Sigma-Aldrich, Saint Louis, MO), rabbit polyclonal di-phosphorylated MLC₂₀
154 (Thr¹⁸/Ser¹⁹) from Dr. M. Seto in Asahi chemical industry (Fuji, Japan), mouse
155 monoclonal anti-calcium channel L-type DHPR alpha subunit (Cav α_2) (cat no. ab2864,
156 Abcam, Cambridge, UK), mouse monoclonal anti-Slo1 (BK α 1) (cat no. MABN70,
157 EMD Millipore, Billerica, MA).

158

159 **Mice**

160 All animal experiments were conducted according to the Fundamental Guidelines
161 for Proper Conduct of Animal Experiment and Related Activities in Academic Research
162 Institutions under the jurisdiction of the Ministry of Education, Culture, Sports, Science

163 and Technology of Japan, and were approved by the Committee on Animal in
164 Kanazawa University. PI3K-C2 α -floxed (C2 α ^{fl/fl}) mice were described previously (14).
165 PI3K-C2 β mice that carry 3 loxP sequences, one loxP before exon 3 and two loxP
166 sequences flanking the neomycin cassette (neo) in the recombinated *Pik3c2b* gene
167 (C2 β ^{3lox/3lox} mice) (Supplementary Fig. 1) (18) were obtained from the Jackson
168 laboratory (B6.129-*Pik3c2b*^{tm1Pkh/J}, stock No. 005702) and described elsewhere (19).
169 To generate mice with *Pik3c2b*-conditional allele that carries two loxP sites (C2 β ^{fl/fl}
170 mice), C2 β ^{3lox/3lox} mice were crossed with Insulin-Cre recombinase (Cre) transgenic
171 mice to delete the neo (Supplementary Fig. 1) (14,18). To generate *Pik3c2b* null (C2 β ^{-/-})
172 mice, 3 loxP-targeted allele was removed by intercrossing the CAG-Cre transgenic mice
173 line (20) (Supplementary Fig. 2) (18). To generate smooth muscle-specific
174 *Pik3c2b*-conditional KO (C2 β ^{fl/fl}; SM22 α -Cre) mice, C2 β ^{fl/fl} mice were crossed with
175 SM22 α -Cre transgenic mice (21) (Supplementary Fig. 1) (18). In some experiments,
176 C2 β ^{3lox/3lox} mice were crossed with SM22 α -Cre transgenic mice to generate smooth
177 muscle-specific C2 β ^{-/-} mice (Supplementary Fig. 3) (18). In the present study, we
178 employed three genetically different mice with C2 α - and C2 β -double KO in smooth
179 muscle, i.e. C2 α ^{fl/fl}; C2 β ^{fl/fl}; SM22 α -Cre, C2 α ^{fl/fl}; C2 β ^{3lox/3lox}; SM22 α -Cre, and C2 α ^{fl/fl};
180 C2 β ^{-/-}; SM22 α -Cre mice (Supplementary Figures 1-3)(18), to study roles of C2 α and

181 C2 β . Rosa26-CAG-loxP-stop-loxP-tdTomato (R26-tdTomato) reporter mice were from
182 the Jackson Laboratory (B6;129S6-*Gt(ROSA)^{26Sortm14(CAG-tdTomato)Hze}/J*, Stock No.
183 007908). SM22 α -Cre; R26-tdTomato mice were generated to evaluate Cre-mediated
184 recombination efficiency. Mice were sacrificed using intraperitoneal injection (*i.p.*) of
185 pentobarbital (Kyoritsu, Tokyo, Japan) overdose according to the acceptable *euthanasia*
186 guidelines. Mice were genotyped by PCR analysis of genomic DNA prepared from tail
187 biopsies.

188

189 **Counting pups and intrauterine fetuses**

190 We performed timed mating of mice. Mouse mating was performed in 1:1 ratio by
191 placing one female mouse into a cage containing one male mouse at late afternoon at
192 gestational day (GD) 0. The following morning, all female mice, whether they were
193 containing vaginal plug or not, were separated from male mice and followed until
194 GD18.5 or delivery. We counted delivered pups on the morning of the expected day of
195 delivery. In some pregnant female mice, we carefully monitored numbers of pups
196 delivered from each mouse every three hours on the expected delivery day. For counting
197 intrauterine fetuses in the fertility test, mice were sacrificed at GD 18.5 with overdose of
198 pentobarbital and intrauterine fetuses were counted. In the fertility test, 12 control and

199 12 double KO mice were used and the data was from 5 litters in both control and
200 smDKO female mice.

201

202 **Western blotting**

203 For preparation of non-stimulated myometrium tissue lysate, myometrium layer was
204 quickly dissected from the isolated uterus by removing the endometrium and placenta
205 after sacrificing mice. The myometrial tissues were snap-frozen by soaking them in
206 liquid nitrogen. Frozen tissues were quickly homogenized with glass homogenizer in ice
207 cold modified RIPA buffer (10 mM Tris-HCl, pH7.4, 100 mM NaCl, 1 mM EDTA,
208 1mM EGTA, 1 mM NaF, 20 mM Na₂HPO₄, 2 mM Na₃VO₄, 0.1% SDS, .05% Sodium
209 deoxycholate, 1% Triton-X 100, 10% glycerol, and one tablet of complete mini per 10
210 ml buffer) or kept at -80°C for storage. After debris was removed, the samples were
211 solubilized in 2 times concentrated Laemmli's SDS sample buffer, boiled for 5 mins,
212 and then separated on 8% or 14% SDS-PAGE, followed by electrotransfer to PVDF
213 membranes (Immobilon-P, Millipore-Merck, Darmstadt, Germany). After blocking with
214 5% bovine serum albumin (BSA) for 1 h, the membranes were incubated overnight with
215 different antibodies at 4 °C, followed by incubation with alkaline
216 phosphatase-conjugated secondary antibodies for 1 h at room temperature. Protein

217 bands were visualized by color reaction using nitro blue tetrazolium/
218 5-bromo-4-choloro-3'-indolyphosphate p-toluidine system. The band densities of
219 different proteins were determined, using Image Studio lite software (LI-COR).

220

221 **Immunofluorescent staining**

222 Cryosections of uterus were stained for immunofluorescence observations, using
223 standard protocol as described previously (14). Briefly, after overnight fixation in 4%
224 PFA in Ca^{2+} and Mg^{2+} free PBS, the tissues were washed several times with PBS,
225 cryoprotected in 20% sucrose for 12-16 h and snap frozen with TissueTek optimal
226 cutting temperature (OCT) compound (Sakura, Tokyo, Japan). Tissue sections (7 μm)
227 were prepared by using Sakura Tissue-Tek Cryo3 and the sections were blocked with
228 5% normal goat serum in 0.3% Triton-X/PBS for 1h at room temperature. Primary
229 antibodies were applied at the indicated dilutions: anti-PI3K-C2 α (1:100), anti-
230 PI3K-C2 β (1:200), anti-Mhc11 (1:250), anti-calcium channel L-type DHPR alpha
231 subunit (Cav α_2) (1:100), anti-Slo1 (BK α 1) (1:150) and incubated for 12-16 h at 4°C.
232 After several washes by PBS, Alexa Fluor 488 conjugated anti-rabbit IgG (1:1000) was
233 applied to the sections and incubated at room temperature for 2h. Sections were
234 counterstained with DAPI for 30 mins and mounted with Fluoromount (Diagnostic

235 BioSystems, Pleasanton, CA) with coverslips. Confocal microscopic observations were
236 carried out on an inverted Nikon Eclipse Ti2 confocal microscope (Nikon Instruments),
237 attached to an Andor Dragonfly spinning-disk unit, Andor EMCCD camera (iXon
238 DU888) (Andor Technologies) and a laser unit (Coherent). An oil-immersion objective
239 (PlanApo 60X, NA 1.4) (Nikon) was used for all experiments. Excitation for DAPI,
240 Alexa488 and Alexa568 chromophores was provided by 405, 488 and 561 nm laser,
241 respectively. Super-resolution imaging of fixed cells was performed using an Andor
242 Dragonfly confocal microscope in SRRF-Stream mode.

243

244 **Measurements of tension and phosphorylation of MLC₂₀ and MYPT1**

245 Tension measurements were performed as described previously (22). In brief,
246 isolated uteri were placed immediately in ice-cold Krebs-Henseleit buffer composed of
247 (in mM) NaCl 119, KCl 4.7, KH₂PO₄ 1.2, MgSO₄ 1.5, CaCl₂ 1.5, NaHCO₃ 25 and
248 glucose 11. The buffer containing uterine tissues was continuously aerated with 95% O₂
249 and 5% CO₂. Uteri were cleaned of fetus, placenta and other adherent tissues and made
250 strips of about 2.5mm x 15mm length. After placing strips in contraction chambers,
251 generated tension was determined isometrically with transducer (UM-203; Kishimoto
252 Medical Instruments, Kyoto, Japan) with continuously aerated by 95% O₂ and 5% CO₂.

253 Before test stimulation, the rings were precontracted with 60 mM KCl containing buffer
254 and poorly responsive strips were not used for analyses. Spontaneous tension and
255 oxytocin- and KCl-induced tension were corrected by the tension generated by the
256 application of a hypotonic buffer at the end of tension measurements as described
257 previously (23,24). The optimal concentrations of oxytocin, Y-27632 and nitrendipine
258 were determined by preliminary experiments.

259 Uterine strips contracted isometrically were fixed in acetone dry ice slurry
260 containing 20 mM dithiothreitol (DTT) and 10% trichloroacetic acid and washed in
261 acetone containing 10mM DTT at room temperature, as described previously (12).
262 Fixed tissues were homogenized in a homogenization buffer comprising 20 mM
263 Tris/HCl (pH 7.5), 100 mM NaF, 1 mM Na₃VO₄, 0.1% SDS, 2 mM EGTA, 0.5%
264 NP-40, 20 µg/ml each of leupeptin and aprotinin and 1 mM PMSF. The homogenates
265 were mixed with 4 times concentrated Laemmli's SDS sample buffer and boiled for 5
266 minutes. The samples (40 µg protein) were separated on 8% and 14% SDS-PAGE,
267 followed by western blot analysis using phospho-MLC₂₀ and -MYPT1 specific
268 antibodies and antibodies that recognize both phospho- and nonphospho-proteins. The
269 amounts of the phospho-proteins quantitated by densitometry were normalized for total
270 amounts of MLC₂₀ and MYPT1 in each sample, and the quantified data of normalized

271 amounts of the phospho-proteins were expressed as multiples over a value in
272 unstimulated tissues, which is expressed as 1.0.

273

274 **Isolation and culture of myometrial cells**

275 Myometrial cells were isolated and cultured as described previously (25). Briefly,
276 the uterus quickly removed from euthanized mice was washed with ice-cold Hank's
277 balanced salt solution (HBSS) and cut through the longitudinal axis. The placenta, fetus
278 and endometrium were removed from the uterus and the myometrium layer was finely
279 chopped with scissors. The myometrial tissues were incubated in 1 unit/ml Liberase-TM
280 in HBSS solution for 1 h at 37 °C. Cell suspension was prepared by gently pipetting
281 15-20 times with penicillin G- and streptomycin-supplemented, 5% FBS-containing
282 advanced DMEM and filtered through 100 µm Cell Strainer (cat no. 352360, Falcon,
283 Corning, NY). Cell suspension was centrifuged at 450 x g for 5 min at 20 °C, and the
284 resultant cell pellet was resuspended in penicillin G- and streptomycin- supplemented,
285 5% FBS-containing advanced DMEM and plated onto type I collagen (Nitta
286 gelatin)-coated dishes.

287

288 **Measurements of the intracellular free Ca²⁺ concentration ([Ca²⁺]_i)**

289 For measurements of the $[Ca^{2+}]_i$, freshly isolated myometrial smooth muscle cells
290 were seeded on type I collagen-coated glass-bottomed culture dishes (cat no.
291 P35G-1.0-14-C, Mat Tek Corp.) and kept for 18-20 h at 37°C in the atmosphere
292 containing 5 % CO₂. Cells were washed with pre-warmed HBSS and loaded by 5 μM of
293 Fluo-8 AM in HBSS for 30 mins. After washing twice by HBSS, cells were incubated in
294 phenol red-free FluoroBrite DMEM (Gibco) on a heated stage chamber at 37 °C
295 temperature and 5% CO₂ atmosphere (Tokai-Hit). The intracellular Ca²⁺-imaging was
296 performed using a customized inverted microscope (IX70, Olympus)-based spinning
297 disk (CSU-10, Yokogawa) confocal system, equipped with an EM-CCD cooled
298 charge-coupled devise camera (iXon, Andor, UK) and a light engine (Lumencor, Inc.).
299 Fluorescent images were captured every 500 ms with excitation at 488 nm light and
300 fluorescence detection at 510 nm. Pixel density was calculated from whole cell averages
301 using the iXon iQ software (Andor). The ratio of oxytocin stimulated peak fluorescence
302 intensity (F) / basal intensity (F₀) was expressed.

303

304 **Determination of Rho activation by fluorescence resonance energy transfer**
305 **(FRET) imaging technique**

306 For FRET imaging analysis, after myometrial smooth muscle cells were isolated,

307 they were transfected with the pRaichu-RhoA probe (26) using an Amaxa Nucleofector
308 system (Lonza) and plated onto type I collagen-coated glass-bottomed culture dishes.
309 Twenty-four h later, the transfected cells were imaged using the same basic confocal
310 microscope system as described for the $[Ca^{2+}]_i$ measurements. For the measurements of
311 Rho-FRET signals, the confocal system was configured with a CFP and YFP filter set
312 (Di01-T445/515/561-13×15×0.5, Semrock). The employed chimeric FRET probe
313 protein consists of N-terminal yellow fluorescent protein (YFP), the Rho-binding
314 domain of PKN, RhoA, and C-terminal cyan fluorescent protein (CFP). When RhoA in
315 the chimeric FRET probe protein is bound to GDP, fluorescence of 475 nm emanates
316 from CFP with excitation at 433 nm. When RhoA is bound to GTP, intramolecular
317 binding of GTP-loaded RhoA to the RBD brings YFP into close proximity to CFP,
318 which causes FRET and fluorescence of 527 nm from YFP. The chimeric FRET
319 probe-transfected cells were stimulated with oxytocin (100 nM), which was added after
320 2 min observations of baseline signals. Pseudo-grayscale ratio images were generated
321 from images from CFP and FRET channels using Andor iQ software. RhoA FRET
322 signals intensity within 4 subcellular regions per cell at 3 min after the additions of
323 oxytocin was quantified. The ratio of oxytocin stimulated fluorescence intensity (F) /
324 basal intensity (F₀) is expressed.

325

326 **Statistics**

327 Statistical analysis and graphical presentation were performed with Prism 7 software

328 (GraphPad Software). Data are presented as means \pm standard error of mean (SEM).

329 Analysis between two groups was done with 2-tailed unpaired Student's *t*-test. For

330 comparison between multiple groups, one or two ways ANOVA followed by Bonferroni

331 post hoc test was used unless stated otherwise. *p* value < 0.05 was considered to be

332 statistically significant.

333

334

335

336

337

338

339

340

341

342

343 **Results**

344 **Genetic deletion of C2 α and C2 β in female mice impedes fetal delivery**

345 In order to study roles of C2 α and C2 β in the smooth muscle organs, we generated
346 smooth muscle-specific KO mice of C2 α and C2 β by mating C2 α - and C2 β -floxed mice
347 with SM22 α -Cre transgenic mice. In this study, we used two different types of
348 C2 β -floxed mice, i.e. C2 β ^{fl/fl} and C2 β ^{3lox/3lox} mice (Supplementary Figs. 1 and 3C) (18),
349 to delete C2 β gene specifically in smooth muscle tissues. We confirmed that SM22 α
350 promoter-driven Cre expression effectively deleted the floxed gene in the
351 R26-tdTomato reporter construct in smooth muscle tissues including uterus and bladder
352 (Fig. 1A). SM22 α promoter-driven Cre expression substantially decreased the protein
353 expression of both C2 α and C2 β in the myometrial layer of the uterus (Fig. 1B) of
354 smDKO mice with the genotype of C2 α ^{fl/fl};C2 β ^{fl/fl};SM22 α -Cre. While we were
355 conducting the mating, we found that female smDKO mice in the mating
356 (C2 α ^{fl/fl};C2 β ^{fl/fl};SM22 α -Cre (female) x C2 α ^{fl/fl};C2 β ^{fl/fl} (male)) delivered reduced
357 numbers of pups compared with two other mating (C2 α ^{fl/fl};C2 β ^{fl/fl} (female) x
358 C2 α ^{fl/fl};C2 β ^{fl/fl};SM22 α -Cre (male), and C2 α ^{fl/fl};C2 β ^{fl/fl} (female) x C2 α ^{fl/fl};C2 β ^{fl/fl} (male))
359 (Table 1). We also observed a reduction in the number of pups from female
360 C2 α ^{fl/fl};C2 β ^{-/-};SM22 α -Cre mice, in which C2 β is globally deleted, compared with female

361 $C2\alpha^{fl/fl};C2\beta^{-/-}$ mice (Table 2). $C2\beta^{3lox/3lox}$ mice expressed approximately 80% of the $C2\beta$
362 protein expression level in smooth muscle tissues of wild-type mice. The pup number
363 from female $C2\alpha^{fl/fl};C2\beta^{3lox/3lox};SM22\alpha-Cre$ mice was also reduced compared with
364 female wild-type and $C2\alpha^{fl/fl};C2\beta^{3lox/3lox}$ mice (Table 3). In contrast, single smooth
365 muscle-specific KO of $C2\alpha$ (sm $C2\alpha$ KO) or $C2\beta$ (sm $C2\beta$ KO) in female mice did not
366 reduce pup numbers (Table 3). We followed the time course of the delivery in pregnant
367 mice: both control ($C2\alpha^{fl/fl};C2\beta^{fl/fl}$) and smDKO mice started delivery at night or early
368 morning. The control mice finished the delivery process by 15:00 whereas smDKO
369 mice delivered the small number of pups by 15:00 and thereafter smDKO mice did not
370 deliver pups or delivered only a few pups by 24:00 (Fig. 1C). Regardless of the
371 decreased pups delivered from smDKO mice, the number of fetuses at gestational day
372 (GD) 18.5 in the uterus of smDKO mice was not different from that of control
373 $C2\alpha^{fl/fl};C2\beta^{fl/fl}$ mice (Fig. 1D). The gross fetal appearance including the attachment and
374 orientation of fetuses to the placenta in smDKO pregnant mice were also similar to that
375 in control mice. These observations suggested that the fetal delivery process was
376 impaired in female smDKO mice.

377

378 **Contraction of uterine smooth muscle from smDKO mice is impaired**

379 The gross structure of the uterus was similar in female control and smDKO mice.
380 The myometrium in the uterus of smDKO mice showed the well-developed outer
381 longitudinal and inner circular layers with normal thickness compared with control
382 $C2\alpha^{fl/fl};C2\beta^{fl/fl}$ mice (Fig. 2 A and B). The endometrium in smDKO mice also appeared
383 normal microscopically compared with control $C2\alpha^{fl/fl};C2\beta^{fl/fl}$ mice (Fig. 2B). In
384 addition, the expression levels of different contractile and smooth muscle specific
385 proteins including smooth muscle-specific myosin heavy chain Mhc11, MLCK, the
386 actin filament-associated caldesmon and calponin, the catalytic subunit of myosin light
387 chain (MLC₂₀) phosphatase PP1 δ and the myosin-binding regulatory subunit of MLC₂₀
388 phosphatase MYPT1 were all similar in the uteri of control and smDKO mice at both the
389 non-pregnant and pregnant (GD18.5) stages (Fig. 2C). The expression of C2 α protein in
390 the myometrium of control mice was also similar at the non-pregnant and pregnant
391 (GD18.5) stages (Fig. 2D). C2 β protein in pregnant control mice tended to be lower
392 compared with non-pregnant control mice. The expression of C2 α and C2 β in smDKO
393 mice was substantially reduced at the non-pregnant and pregnant stages compared with
394 control mice.

395 We next studied the possibility that smDKO pregnant mice might have impaired
396 uterine contraction, which led to the impeded delivery. We prepared uterine strips from

397 control and KO mice at GD18.5 and compared contractile responses. The uterine strips
398 showed spontaneous, repeated contraction of the duration of several seconds under the
399 isometric condition. The amplitude and frequency of spontaneous contraction were both
400 reduced in uterine strips from smDKO mice compared with those from control mice
401 (Fig. 3A upper and Fig. 3A lower). The uterine strips from single C2 α KO (smC2 α KO)
402 mice showed similar amplitudes and frequency of spontaneous contraction to those of
403 control mouse strips. The uterine strips from single C2 β KO (smC2 β KO) mice showed
404 similar amplitude, but lower frequency of spontaneous contraction compared with
405 control mice. Similar to the case of spontaneous contraction, the amplitudes of
406 contractile responses induced by oxytocin and KCl, which activate phospholipase
407 C/Rho pathways and L-type voltage-dependent Ca²⁺ channel, respectively, were also
408 diminished in smDKO but not smC2 α KO and smC2 β KO uterine strips compared with
409 control mice (Fig. 3 B and C). Oxytocin and KCl increased spike frequency to the
410 similar extents in control, smC2 α KO, smC2 β KO and smDKO strips (lower panels of
411 Fig. 3B and C), compared with oxytocin- and KCl-nonstimulated strips (lower panel of
412 Fig. 3A).

413 To explore the mechanisms by which uterine contraction is dependent on C2 α and
414 C2 β , we compared the responses of uterine contraction to the L-type voltage-dependent

415 Ca^{2+} channel antagonist nitrendipine and the Rho kinase inhibitor Y-27632 in control
416 and smDKO strips. Nitrendipine substantially inhibited spontaneous contraction in both
417 control and smDKO strips. Nitrendipine relatively weakly inhibited oxytocin-induced
418 contraction in control and smDKO strips compared with spontaneous contraction. These
419 observations suggest that both L-type Ca^{2+} channel-dependent and -independent
420 mechanisms are involved in spontaneous and oxytocin-induced contraction in control
421 and smDKO uterine smooth muscle. The amplitudes of spontaneous and
422 oxytocin-induced contraction in the presence of nitrendipine were similar in control and
423 smDKO strips (Fig. 3D). These results may suggest that L-type Ca^{2+} channel-dependent
424 contraction involves both $\text{C2}\alpha/\text{C2}\beta$ -dependent and -independent contractile
425 mechanisms whereas L-type Ca^{2+} channel-independent contraction does not require
426 $\text{C2}\alpha$ or $\text{C2}\beta$. Y-27632 partially inhibited spontaneous- and oxytocin-induced
427 contraction in control strips, but did not significantly inhibit contraction of smDKO
428 strips (Fig. 3E), suggesting that both Rho kinase-dependent and -independent contractile
429 mechanisms are involved in spontaneous and oxytocin-induced contraction in control
430 strips. In contrast, contraction of smDKO uterine smooth muscle is largely Rho
431 kinase-independent. It is suggested that Rho kinase-dependent contraction requires $\text{C2}\alpha$
432 and $\text{C2}\beta$ whereas Rho kinase-independent one does not.

433

434 **Oxytocin-induced phosphorylation of MLC₂₀ and MYPT1 is attenuated in uterine**
435 **smooth muscle tissues of smDKO mice**

436 We compared oxytocin-induced phosphorylation of MLC₂₀ and MYPT1, the latter
437 phosphorylation of which inhibits MLC₂₀ phosphatase to lead to an increase in MLC₂₀
438 phosphorylation, in uterine strips of smDKO and control mice. Oxytocin induced a
439 1.6-fold increase in mono-phosphorylation (Ser¹⁹) of MLC₂₀ (p-MLC₂₀) in uterine
440 strips of control mice, but not in those of smDKO mice (Fig. 4A). Oxytocin also
441 induced a 2.6-fold increase in di-phosphorylation (Thr¹⁸/Ser¹⁹) of MLC₂₀ (pp-MLC₂₀),
442 which is known to be increased when MLC₂₀ phosphatase is inhibited or MLCK
443 activity becomes very high (27) , in control mouse uterine strips (Fig. 4B). In contrast,
444 in smDKO mouse strips, oxytocin did not increase pp-MLC₂₀ level above that in the
445 non-stimulated control strips. Furthermore, oxytocin induced a 2.0-fold increase in
446 phosphorylation (Thr⁸⁵³) of the myosin light chain₂₀ phosphatase (MLCP)-regulatory
447 subunit MYPT1, which results in inhibition of MLCP, in control mouse strips but not in
448 smDKO mouse strips (Fig. 4C). Thus, both mono- and di-phosphorylation levels of
449 MLC₂₀ are reduced with diminished inhibition of MLCP in smDKO mouse strips.

450

451 **Rho signaling but not Ca²⁺ signaling is downregulated in smDKO myometrial cells**

452 We isolated myometrial cells from control and smDKO pregnant mice. The
453 morphology of the isolated cells observed under bright field microscopy was similar
454 between control and smDKO mice (Fig. 5A). We identified 70 % of the isolated cells as
455 smooth muscle, using mice that expressed td-Tomato reporter gene specifically in
456 smooth muscle (Fig. 5B).

457 We determined oxytocin-induced changes in the [Ca²⁺]_i in isolated myometrial
458 smooth muscle. Oxytocin induced similar extents (approximately 6-fold) of the peak
459 increases in the [Ca²⁺]_i in both control and smDKO myometrial smooth muscle (Fig.
460 5C). Because uterine smooth muscle contraction is dependent on L-type Ca²⁺ channels,
461 we analyzed the protein expression of the α_2 subunit (Cav _{α_2}) of L-type calcium channel
462 in control and smDKO mice uterus. The expression level of Cav _{α_2} protein in the uterus
463 was similar in control and smDKO mice as evaluated by Western blotting (Fig. 5D).
464 Immunofluorescence of the uterine tissues with anti-Cav _{α_2} antibody showed that the
465 myometrial smooth muscle in both control and smDKO uterus expressed this protein
466 (Fig. 5E, left). With SRRF microscopy, we obtained higher resolution views of the
467 immunostained myometrial layer, which showed that Cav _{α_2} was distributed mainly on
468 the plasma membrane or its vicinity of smooth muscle (Fig. 5E left). BK channel, which

469 is a negative regulator of L-type calcium channels, was also distributed largely on the
470 plasma membrane or its vicinity of smooth muscle, and there was no detectable
471 difference of BK channel expression in control and smDKO mouse uterus (Fig. 5E
472 right).

473 The phosphorylation of MYPT1, which is controlled mainly by Rho kinase
474 downstream of Rho, was decreased in smDKO uterine smooth muscle (Fig. 4C).
475 Therefore, we determined oxytocin-induced Rho activation in isolated myometrial
476 smooth muscle cells, using a FRET imaging technique. In control smooth muscle cells,
477 we observed substantial oxytocin-induced Rho activation signals at the plasma
478 membrane and the intracellular compartment. In smDKO myometrial smooth muscle
479 cells, Rho activation signals at both the plasma membrane and the intracellular
480 compartment were diminished (Fig. 5F).

481

482

483

484

485

486

487 **Discussion**

488 In parturition, the uterine smooth muscle develops potent contractile force to expel
489 the fetus. Dramatic changes in the signaling and contractile machineries of uterine
490 smooth muscle as well as the neuroendocrine functions at the end of pregnancy allows
491 generation of potent uterine contraction at parturition (1,2,28,29) . In the present study,
492 we identified the novel smooth muscle molecules, class II PI3K C2 α and C2 β , which
493 are required for full contraction of uterine smooth muscle and normal delivery. C2 α and
494 C2 β are involved in activation of Rho and resultant Rho-kinase-dependent inhibition of
495 MLCP, which potentiates MLC₂₀ phosphorylation and contractile force in uterine
496 smooth muscle (27-31) . Highly homologous C2 α and C2 β completely compensate for
497 the effects of single gene deletion of each other in parturition, and only double KO
498 results in defects in parturition.

499 In uterine smooth muscle, activation of cell surface receptors including oxytocin and
500 prostaglandin F_{2 α} and Ca²⁺ channels including the L-type voltage-dependent Ca²⁺
501 channels triggers an increase in [Ca²⁺]_i by Ca²⁺ release from the intracellular Ca²⁺ store
502 and Ca²⁺ entry through the plasma membrane Ca²⁺ channels (28,30,32) . The increase in
503 the [Ca²⁺]_i activates Ca²⁺/calmodulin-dependent MLCK (Ca²⁺-MLCK pathway),
504 leading to MLC₂₀ phosphorylation and smooth muscle contraction. Oxytocin and

505 prostaglandin $F_{2\alpha}$ also activate small GTPase Rho via the heterotrimeric G protein
506 $G_{12/13}$ (28,30,31). Rho activates its effector Rho kinase, resulting in inhibition of MLCP
507 by phosphorylating the regulatory subunit of MLCP, MYPT1 (Rho-Rho kinase-MLCP
508 pathway) (27). Inhibition of MLCP potentiates MLCK-catalyzed MLC_{20}
509 phosphorylation and contraction. Therefore, Rho-MLCP pathway as well as
510 Ca^{2+} -MLCK pathway coordinately and effectively increase MLC_{20} phosphorylation,
511 thus playing a critical role in oxytocin-induced uterine smooth muscle contraction
512 (28-31,33,34) . The Ca^{2+} signaling pathway and Rho-Rho kinase signaling pathways
513 may have cross-communication because it was reported that Ca^{2+} entry across the
514 plasma membrane activated Rho and Rho kinase in several different types of smooth
515 muscle and that Rho kinase activated voltage-dependent Ca^{2+} channels through
516 phosphorylation (22,23,35) . Importantly, the uterine smooth muscle in the late
517 pregnancy has increased oxytocin receptor number and the depolarization of the resting
518 membrane potential, which increase excitability and contraction of uterine smooth
519 muscle (28,29,31-34).

520 The contraction data in the present study showed that not only oxytocin-induced
521 contraction but also spontaneous and KCl membrane depolarization-induced contraction
522 was attenuated in smDKO uterine smooth muscle compared with control smooth muscle.

523 Mechanistically, spontaneous and membrane depolarization-induced contraction as well
524 as oxytocin-induced contraction were inhibited by a Rho kinase inhibitor, suggesting the
525 contribution of Rho kinase pathway to these contractile responses in control mice.
526 Notably, the extents of contraction inhibition by a Rho kinase inhibitor were marginal in
527 smDKO uterine smooth muscle, suggesting that the contribution of Rho kinase pathway
528 to contraction was greatly diminished in smDKO smooth muscle. The decreased
529 MYPT1 phosphorylation and MLC₂₀ di-phosphorylation in oxytocin-stimulated smooth
530 muscle supported this notion (27). The direct measurements of Rho activation in the
531 myometrial cells by the FRET imaging technique showed that oxytocin-induced Rho
532 activation was decreased in smDKO myometrial cells. Thus, it is likely that the
533 decreased Rho activity results in a higher MLCP activity, leading to reductions in
534 MLC₂₀ phosphorylation and contraction in smDKO smooth muscle. These data also
535 suggest in smDKO smooth muscle that decreased Rho kinase activity might induce
536 diminished activation of L-type Ca²⁺ channels and, thereby, reduced spontaneous and
537 KCl-induced contraction (35).

538 In our previous study (14), we found that VEGF-induced Rho activation occurred in
539 the intracellular endosomal compartment, in which the internalized VEGF receptor-2
540 resided in endothelial cells. Both processes of the VEGF receptor-2 internalization and

541 endosomal Rho activation required C2 α . We also observed that C2 α is required for the
542 endosomal signaling induced by other receptor ligands including S1P and TGF β 1 (9,15).
543 The catalytic product of C2 α , PI(3,4)P₂, contributes to endocytosis by recruiting various
544 PI(3,4)P₂-binding domain-containing proteins, which include SNX9, and promoting
545 clathrin-coated vesicle formation (36) . A role of C2 β in endocytosis is currently almost
546 unknown. Since C2 α single KO did not impair uterine smooth muscle contraction, very
547 likely C2 β can compensate for a defect caused by C2 α deficiency in uterine smooth
548 muscle. In smDKO uterine smooth muscle, the amount of PI(3,4)P₂ produced by
549 slightly expressed C2 α and C2 β is probably insufficient for receptor internalization and
550 subsequent signaling in the endosomes in which receptors and their associated signaling
551 molecules are assembled. A special form of Rho-guanine nucleotide exchange factor
552 (Rho-GEF) is implicated in Rho activation in the endosomes (37,38). The Rho-GEF,
553 Syx, which was found to be involved in VEGF-induced regulation of cell junctions, is
554 one of the candidate Rho-GEFs. Further studies are required for identifying a Rho-GEF
555 involved in endosomal Rho activation and clarifying the mechanism of recruitment and
556 activation of a Rho-GEF.

557 Because RhoA-Rho kinase-MLCP pathway is a major contractile mechanism in
558 spontaneous and uterotinin-induced contraction (28), the new role of these two class II

559 PI3K isoforms in Rho-Rho kinase-MLCP pathway may provide some insight about the
560 mechanisms for clinical conditions of abnormal uterine contraction including preterm
561 labor, uterine inertia and life-threatening postpartum hemorrhage. For preterm labor,
562 tocolytic agents are administered (39). Administration of class II PI3K inhibitors, which
563 inhibit Rho and thereby stimulate MLCP in uterine smooth muscle, may be candidates
564 for developing new tocolytic agents. On the contrary, for clinical conditions of
565 insufficient uterine contraction such as uterine inertia and life-threatening postpartum
566 hemorrhage, stimulators of class II PI3Ks may bring about beneficial outcome by
567 increasing Rho activity and thereby inhibiting MLCP activity with augmented uterine
568 contraction. The inhibitory and stimulatory mechanisms of C2 α and C2 β at cellular
569 levels are currently not well understood. Therefore, further studies are required to
570 unravel the regulatory mechanism of human class II PI3K activity.

571 In summary, our study showed the importance of the novel molecules, C2 α and
572 C2 β , in the regulation of the Rho-Rho kinase-MLCP pathway and their requirement for
573 full contraction of uterine smooth muscle and parturition. It could be possible that
574 dysfunctions of class II PI3K might lead to clinical conditions caused by abnormal
575 uterine smooth muscle contraction. Further studies are required to explore the detailed
576 mechanisms of class II PI3K actions and the regulation of their activity, which provides

577 further insight into the physiological and pathophysiological roles of class II PI3Ks.

578

579

580 **Acknowledgements**

581 We thank Ms. Chiemi Hirose for secretarial assistance.

582

583

584

585

586

587

588

589

590

591

592

593

594

595 **References**

- 596 **1.** Smith R. Parturition. *N Engl J Med* 2007; 356:271-283
- 597 **2.** Challis JRG, Matthews SG, Gibb W, Lye SJ. Endocrine and paracrine regulation
598 of birth at term and preterm. *Endocr Rev* 2000; 21:514-550
- 599 **3.** Berne RM, Levy MN, Koeppen BM, Stanton BA. *Physiology*. Elsevier Science
600 Health Science Division.
- 601 **4.** Wray S. Insights into the uterus. *Exp Physiol* 2007; 92:621-631
- 602 **5.** Sigger JN, Harding R, Jenkin G. Relationship between electrical activity of the
603 uterus and surgically isolated myometrium in the pregnant and nonpregnant ewe.
604 *J Reprod Fertil* 1984; 70:103-114
- 605 **6.** Thorpe LM, Yuzugullu H, Zhao JJ. PI3K in cancer: divergent roles of isoforms,
606 modes of activation and therapeutic targeting. *Nat Rev Cancer* 2015; 15:7-24
- 607 **7.** Posor Y, Eichhorn-Gruenig M, Puchkov D, Schoneberg J, Ullrich A, Lampe A,
608 Muller R, Zarbakhsh S, Gulluni F, Hirsch E, Krauss M, Schultz C, Schmoranzer
609 J, Noe F, Haucke V. Spatiotemporal control of endocytosis by
610 phosphatidylinositol-3,4-bisphosphate. *Nature* 2013; 499:233-237
- 611 **8.** Marat AL, Wallroth A, Lo WT, Muller R, Norata GD, Falasca M, Schultz C,
612 Haucke V. mTORC1 activity repression by late endosomal phosphatidylinositol

- 613 3,4-bisphosphate. *Science* 2017; 356:968-972
- 614 **9.** Aki S, Yoshioka K, Okamoto Y, Takuwa N, Takuwa Y. Phosphatidylinositol
615 3-kinase class II alpha-isoform PI3K-C2alpha is required for transforming
616 growth factor beta-induced Smad signaling in endothelial cells. *J Biol Chem*
617 2015; 290:6086-6105
- 618 **10.** Falasca M, Maffucci T. Regulation and cellular functions of class II
619 phosphoinositide 3-kinases. *Biochem J* 2012; 443:587-601
- 620 **11.** Yoshioka K, Sugimoto N, Takuwa N, Takuwa Y. Essential role for class II
621 phosphoinositide 3-kinase alpha-isoform in Ca²⁺-induced, Rho- and Rho
622 kinase-dependent regulation of myosin phosphatase and contraction in isolated
623 vascular smooth muscle cells. *Mol Pharmacol* 2007; 71:912-920
- 624 **12.** Wang Y, Yoshioka K, Azam MA, Takuwa N, Sakurada S, Kayaba Y, Sugimoto N,
625 Inoki I, Kimura T, Kuwaki T, Takuwa Y. Class II phosphoinositide 3-kinase
626 alpha-isoform regulates Rho, myosin phosphatase and contraction in vascular
627 smooth muscle. *Biochem J* 2006; 394:581-592
- 628 **13.** Azam MA, Yoshioka K, Ohkura S, Takuwa N, Sugimoto N, Sato K, Takuwa Y.
629 Ca²⁺-independent, inhibitory effects of cyclic adenosine 5'-monophosphate on
630 Ca²⁺ regulation of phosphoinositide 3-kinase C2alpha, Rho, and myosin

- 631 phosphatase in vascular smooth muscle. *J Pharmacol Exp Ther* 2007;
632 320:907-916
- 633 **14.** Yoshioka K, Yoshida K, Cui H, Wakayama T, Takuwa N, Okamoto Y, Du W, Qi
634 X, Asanuma K, Sugihara K, Aki S, Miyazawa H, Biswas K, Nagakura C, Ueno
635 M, Iseki S, Schwartz RJ, Okamoto H, Sasaki T, Matsui O, Asano M, Adams RH,
636 Takakura N, Takuwa Y. Endothelial PI3K-C2alpha, a class II PI3K, has an
637 essential role in angiogenesis and vascular barrier function. *Nat Med* 2012;
638 18:1560-1569
- 639 **15.** Biswas K, Yoshioka K, Asanuma K, Okamoto Y, Takuwa N, Sasaki T, Takuwa Y.
640 Essential role of class II phosphatidylinositol-3-kinase-C2alpha in sphingosine
641 1-phosphate receptor-1-mediated signaling and migration in endothelial cells. *J*
642 *Biol Chem* 2013; 288:2325-2339
- 643 **16.** Jean S, Kiger AA. Classes of phosphoinositide 3-kinases at a glance. *J Cell Sci*
644 2014; 127:923-928
- 645 **17.** Nagumo H, Sasaki Y, Ono Y, Okamoto H, Seto M, Takuwa Y. Rho kinase
646 inhibitor HA-1077 prevents Rho-mediated myosin phosphatase inhibition in
647 smooth muscle cells. *Am J Physiol Cell Physiol* 2000; 278:C57-65
- 648 **18.** Sarker MAK, Aki S, Yoshioka K, Kouji K, Okamoto Y, Ishimaru K, Takuwa N,

649 Takuwa Y. Class II PI3K α and β are required for Rho-dependent uterine smooth
650 muscle contraction and parturition in mice. 2018;
651 https://figshare.com/articles/Supplementary_Figures_pdf/7320227/4

652 **19.** Harada K, Truong AB, Cai T, Khavari PA. The class II phosphoinositide
653 3-kinase C2beta is not essential for epidermal differentiation. *Mol Cell Biol*
654 2005; 25:11122-11130

655 **20.** Matsumura H, Hasuwa H, Inoue N, Ikawa M, Okabe M. Lineage-specific cell
656 disruption in living mice by Cre-mediated expression of diphtheria toxin A chain.
657 *Biochem Biophys Res Commun* 2004; 321:275-279

658 **21.** Li L, Miano JM, Mercer B, Olson EN. Expression of the SM22alpha promoter
659 in transgenic mice provides evidence for distinct transcriptional regulatory
660 programs in vascular and visceral smooth muscle cells. *J Cell Biol* 1996;
661 132:849-859

662 **22.** Sakurada S, Takuwa N, Sugimoto N, Wang Y, Seto M, Sasaki Y, Takuwa Y.
663 Ca²⁺-dependent activation of Rho and Rho kinase in membrane
664 depolarization-induced and receptor stimulation-induced vascular smooth
665 muscle contraction. *Circ Res* 2003; 93:548-556

666 **23.** Janssen LJ, Tazzeo T, Zuo J, Pertens E, Keshavjee S. KCl evokes contraction of

667 airway smooth muscle via activation of RhoA and Rho-kinase. *Am J Physiol*
668 *Lung Cell Mol Physiol* 2004; 287:L852-858

669 **24.** Fischer DP, Hutchinson JA, Farrar D, O'Donovan PJ, Woodward DF, Marshall
670 KM. Loss of prostaglandin F₂α, but not thromboxane, responsiveness in
671 pregnant human myometrium during labour. *J Endocrinol* 2008; 197:171-179

672 **25.** Ying L, Becard M, Lyell D, Han X, Shortliffe L, Husted CI, Alvira CM,
673 Cornfield DN. The transient receptor potential vanilloid 4 channel modulates
674 uterine tone during pregnancy. *Sci Transl Med* 2015; 7:319ra204

675 **26.** Yoshizaki H, Ohba Y, Kurokawa K, Itoh RE, Nakamura T, Mochizuki N,
676 Nagashima K, Matsuda M. Activity of Rho-family GTPases during cell division
677 as visualized with FRET-based probes. *J Cell Biol* 2003; 162:223-232

678 **27.** Somlyo AP, Somlyo AV. Ca²⁺ sensitivity of smooth muscle and nonmuscle
679 myosin II: modulated by G proteins, kinases, and myosin phosphatase. *Physiol*
680 *Rev* 2003; 83:1325-1358

681 **28.** Arthur P, Taggart MJ, Mitchell BF. Oxytocin and parturition: a role for increased
682 myometrial calcium and calcium sensitization? *Front Biosci* 2007; 12:619-633

683 **29.** Wray S, Burdyga T, Noble D, Noble K, Borysova L, Arrowsmith S. Progress in
684 understanding electro-mechanical signalling in the myometrium. *Acta Physiol*

- 685 (Oxf) 2015; 213:417-431
- 686 **30.** Buxton IL. Regulation of uterine function: a biochemical conundrum in the
687 regulation of smooth muscle relaxation. *Mol Pharmacol* 2004; 65:1051-1059
- 688 **31.** Aguilar HN, Mitchell BF. Physiological pathways and molecular mechanisms
689 regulating uterine contractility. *Hum Reprod Update* 2010; 16:725-744
- 690 **32.** Gimpl G, Fahrenholz F. The oxytocin receptor system: structure, function, and
691 regulation. *Physiol Rev* 2001; 81:629-683
- 692 **33.** Tahara M, Morishige K, Sawada K, Ikebuchi Y, Kawagishi R, Tasaka K, Murata
693 Y. RhoA/Rho-kinase cascade is involved in oxytocin-induced rat uterine
694 contraction. *Endocrinology* 2002; 143:920-929
- 695 **34.** Moran CJ, Friel AM, Smith TJ, Cairns M, Morrison JJ. Expression and
696 modulation of Rho kinase in human pregnant myometrium. *Mol Hum Reprod*
697 2002; 8:196-200
- 698 **35.** Yatani A, Irie K, Otani T, Abdellatif M, Wei L. RhoA GTPase regulates L-type
699 Ca²⁺ currents in cardiac myocytes. *Am J Physiol Heart Circ Physiol* 2005;
700 288:H650-659
- 701 **36.** Wallroth A, Haucke V. Phosphoinositide conversion in endocytosis and the
702 endolysosomal system. *J Biol Chem* 2018; 293:1526-1535

- 703 **37.** Ngok SP, Geyer R, Liu M, Kourtidis A, Agrawal S, Wu C, Seerapu HR,
704 Lewis-Tuffin LJ, Moodie KL, Huvelde D, Marx R, Baraban JM, Storz P,
705 Horowitz A, Anastasiadis PZ. VEGF and Angiopoietin-1 exert opposing effects
706 on cell junctions by regulating the Rho GEF Syx. *J Cell Biol* 2012;
707 199:1103-1115
- 708 **38.** Wu C, Horowitz A. Membrane traffic as a coordinator of cell migration and
709 junction remodeling. *Commun Integr Biol* 2011; 4:703-705
- 710 **39.** Jorgensen JS, Weile LK, Lamont RF. Preterm labor: current tocolytic options for
711 the treatment of preterm labor. *Expert Opin Pharmacother* 2014; 15:585-588
712
713
714
715
716
717
718
719
720

721 **Figure Legends**

722 **Figure 1.** Impaired pup delivery in smooth muscle-specific C2 α - and C2 β -double KO
723 mice. (A) Immunofluorescent staining of myosin heavy chain 11 (Mhc11) in the smooth
724 muscle layer of uterus and bladder in SM22 α -Cre;ROSA26-tdTomato reporter mice.
725 Mhc11-positive cells express tdTomato protein. Schematic for the generation of mice
726 with smooth muscle-specific expression of tdTomato fluorescent protein is shown on
727 the top. (B) Immunofluorescent staining of C2 α and C2 β in the uterine myometrium of
728 control and smDKO pregnant mice at gestational day (GD) 18.5. M, myometrium. EM,
729 endometrium. (C) Time-course of the pup delivery from control and smDKO female
730 mice. (D) The uteri of pregnant mice and the numbers of pups within the uteri at GD
731 18.5. The magnified views of the boxed portion of the uteri in the most left pictures are
732 shown in (i) and (ii). In (C) and (D), the numbers in the blanket denote the numbers of
733 analyzed pregnant mice. The data in Fig. 1C and D are expressed as means \pm SE. * p
734 < 0.05.

735

736 **Figure 2.** No abnormality in uterine morphology and smooth muscle-specific protein
737 expression in control and C2 α - and C2 β -double KO mice. (A) Gross views of the uteri
738 of control and smDKO non-pregnant mice. (B) HE staining of uterine sections of

739 control and smDKO non-pregnant mice and myometrial thickness of control and
740 smDKO mice. The representative histological images (left) and quantified data (right).
741 (C) Expression of various smooth muscle-specific proteins in the myometrial tissues of
742 non-pregnant and pregnant (GD18.5) control and smDKO mice (top). The
743 representative western blots (top) and quantified data (bottom). (D) Expression of C2 α
744 and C2 β proteins in the myometrial tissues of non-pregnant and pregnant (GD18.5)
745 control and smDKO mice (top). The representative western blots (top) and quantified
746 data (bottom). In (B) and (D), the numbers in the blanket denote the numbers of
747 analyzed mice. The data in Fig. 2B, C and D are expressed as means \pm SE. * p <
748 0.05 and ** p < 0.01.

749

750 **Figure 3.** Diminished contractile responses with reduced Rho kinase dependence in
751 uterine smooth muscle of C2 α - and C2 β -double KO mice. The isometric tension was
752 determined in the uterine strips from control, single smKO (smC2 α KO and smC2 β KO)
753 mice, and smDKO mice. The amplitudes and frequency of spontaneous contraction (A),
754 KCl-induced contraction (B), and oxytocin-induced contraction (C). The uterine strips
755 were stimulated with 200 nM oxytocin or 60 mM KCl or unstimulated, and maximal
756 tensions and spike frequency were determined. (D) Reductions of contraction by the

757 L-type Ca²⁺ channel antagonist nitrendipine (NTD). The amplitudes and frequency of
758 spontaneous contraction and amplitudes of oxytocin-induced contraction were
759 determined with or without NTD (100 nM) pretreatment as described in “Materials and
760 Methods”. (E) Reductions of contraction by the Rho kinase inhibitor Y27632. The
761 amplitudes and frequency of spontaneous contraction and amplitudes of
762 oxytocin-induced contraction were determined with or without Y27632 (10 μM)
763 pretreatment as described in “Materials and Methods”. In (A) to (E), the numbers in the
764 blanket denote the numbers of analyzed strips. The data are expressed as means ± SE.
765 * p < 0.05, ** p < 0.01 and ***p < 0.001.

766

767 **Figure 4.** Diminished oxytocin-induced phosphorylation of 20 kDa myosin light chain
768 and MYPT1 in uterine smooth muscle of C2α- and C2β-double KO mice.

769 The uterine smooth muscle strips isometrically contracted in response to oxytocin (200
770 nM) stimulation were snap-frozen and analyzed for phosphorylation of MLC₂₀ at Ser¹⁹
771 (p-MLC₂₀) (A) and at Thr¹⁸/Ser¹⁹ (pp-MLC₂₀) (B), and MYPT1 (p-MYPT1) at Thr⁸⁵³
772 (C). The uterine smooth muscle strips were frozen at 3, 10 and 10 min, respectively,
773 after oxytocin addition for the determinations of p-MLC₂₀, pp-MLC₂₀, and p-MYPT1.
774 In (A) to (C), the numbers in the blanket denote the numbers of analyzed samples. The

775 data are expressed as means \pm SE. * $p < 0.05$ and ** $p < 0.01$.

776

777 **Figure 5.** Diminished oxytocin-induced Rho activation, but not intracellular Ca^{2+}
778 mobilization or Ca^{2+} channel protein expression, in myometrial smooth muscle cells
779 from $\text{C2}\alpha$ - and $\text{C2}\beta$ -DKO mice. Myometrial smooth muscle cells were isolated from
780 control and DKO mice. (A) The phase-contrast images of myometrial smooth muscle
781 cells. (B) Smooth muscle-specific expression of tdTomato fluorescent protein in mice
782 that carries R26-tdTomato reporter construct. Nuclei were stained with DAPI. (C)
783 Oxytocin-induced increase in the $[\text{Ca}^{2+}]_i$ in uterine smooth muscle cells from control
784 and smDKO mice. Cells were stimulated with 100 nM oxytocin. The quantified data
785 show the $[\text{Ca}^{2+}]_i$ peak response from 21 control and 20 smDKO cells. (D) Western
786 blotting of L-type Ca^{2+} channel protein $\text{Cav}\alpha_2$ in uterine smooth muscle cells from
787 control and smDKO mice. (E) Immunofluorescent staining of the Ca^{2+} channel $\text{Cav}\alpha_2$
788 and the K^+ channel $\text{BK}\alpha_1$ in the myometrium of control and smDKO mice. The boxed
789 regions were shown as the magnified views obtained with SRRF microscopy, “M”,
790 myometrial layer of uterus. The red arrowheads denote $\text{Cav}\alpha_2$ protein of L-type Ca^{2+}
791 channel in the first SRRF view panel (left) and $\text{BK}\alpha_1$ protein of K^+ channel of last
792 SRRF view panel (right). (F) FRET imaging of Rho activation in uterine smooth muscle

793 cells from control and smDKO mice. Left, representative images of Rho-FRET signals.
794 Right, quantified data from 9 control and 9 smDKO cells. The peak/basal signal ratio in
795 control cells were expressed as 100%. Red arrowhead denotes rho activation signal. In
796 (C), (D) to (F), the numbers in the blanket denote the numbers of analyzed samples. The
797 data in Fig. 5C, D and F are expressed as means \pm SE. ***p < 0.001.

798

799

800

801

802

803

804

805

806

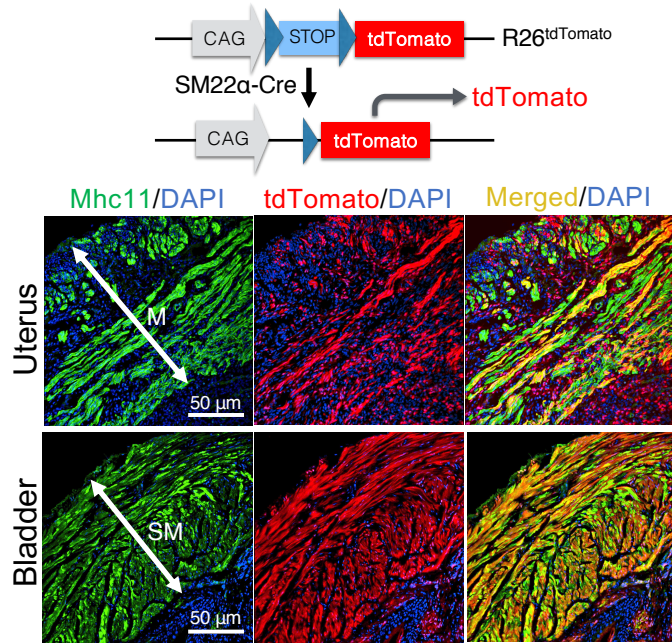
807

808

809

810

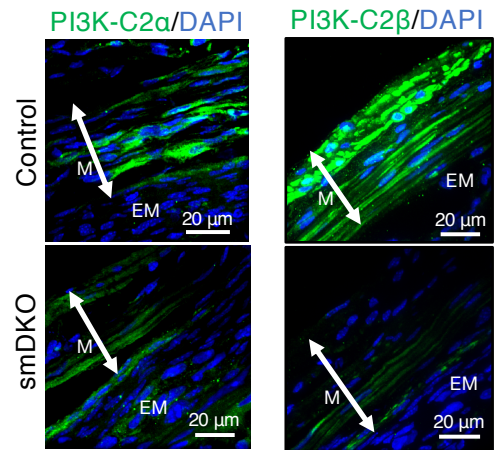
A SM22 α -Cre ; R26^{tdTomato}



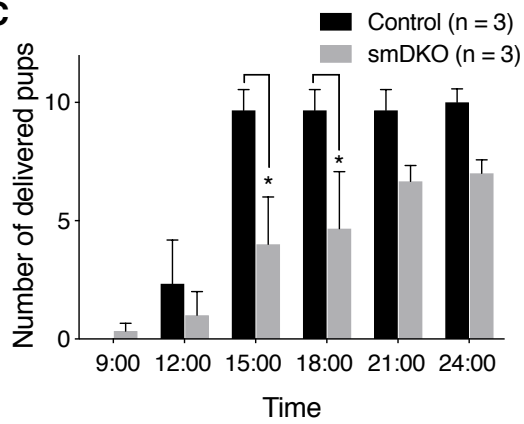
B

Control (female): C2 α ^{fl/fl}; C2 β ^{fl/fl}

smDKO (female): C2 α ^{fl/fl}; C2 β ^{fl/fl}; SM22 α -Cre



C



D

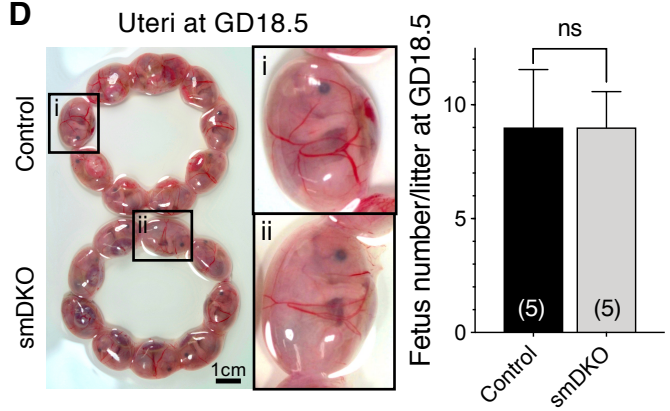


Fig. 1

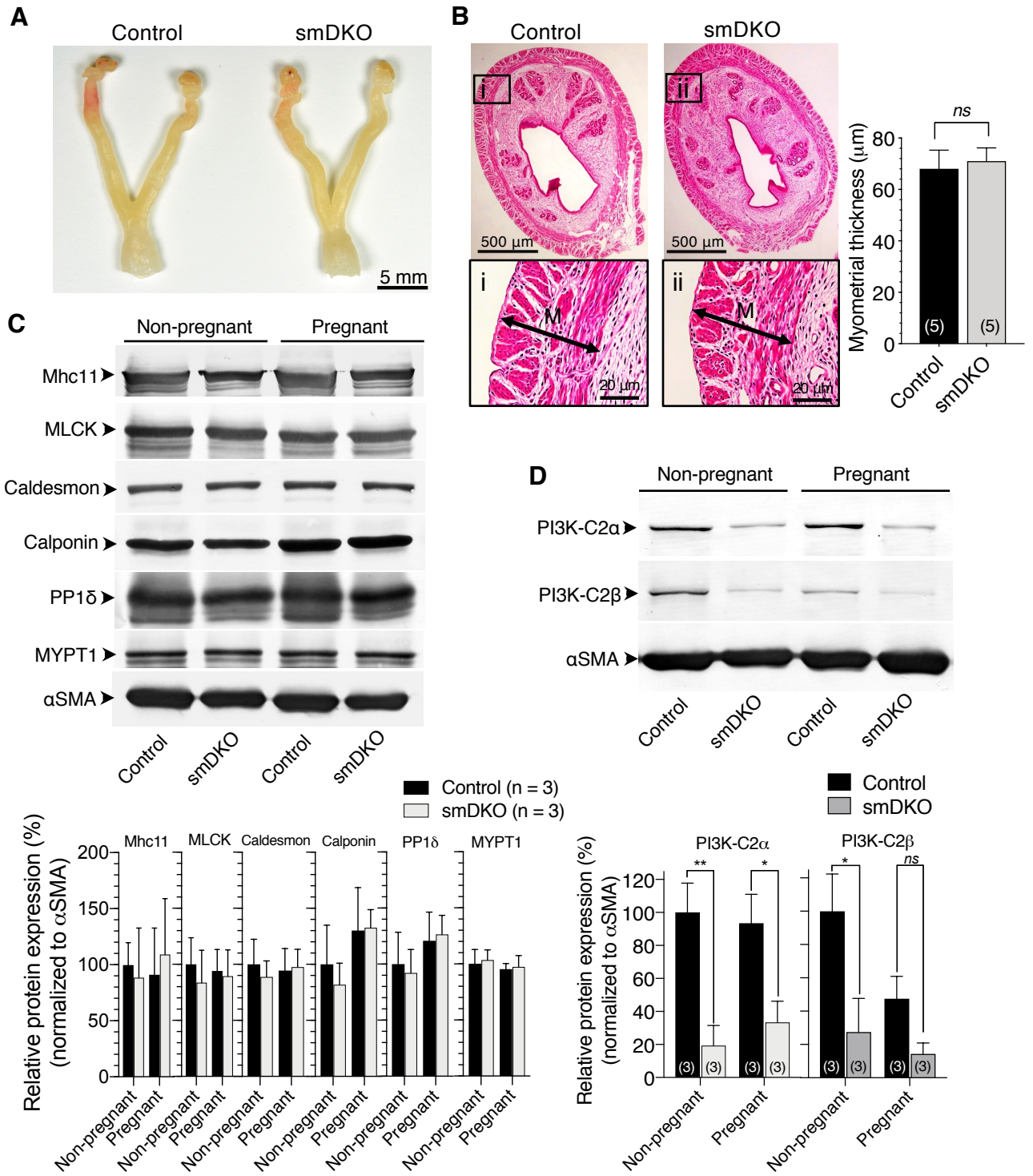


Fig. 2

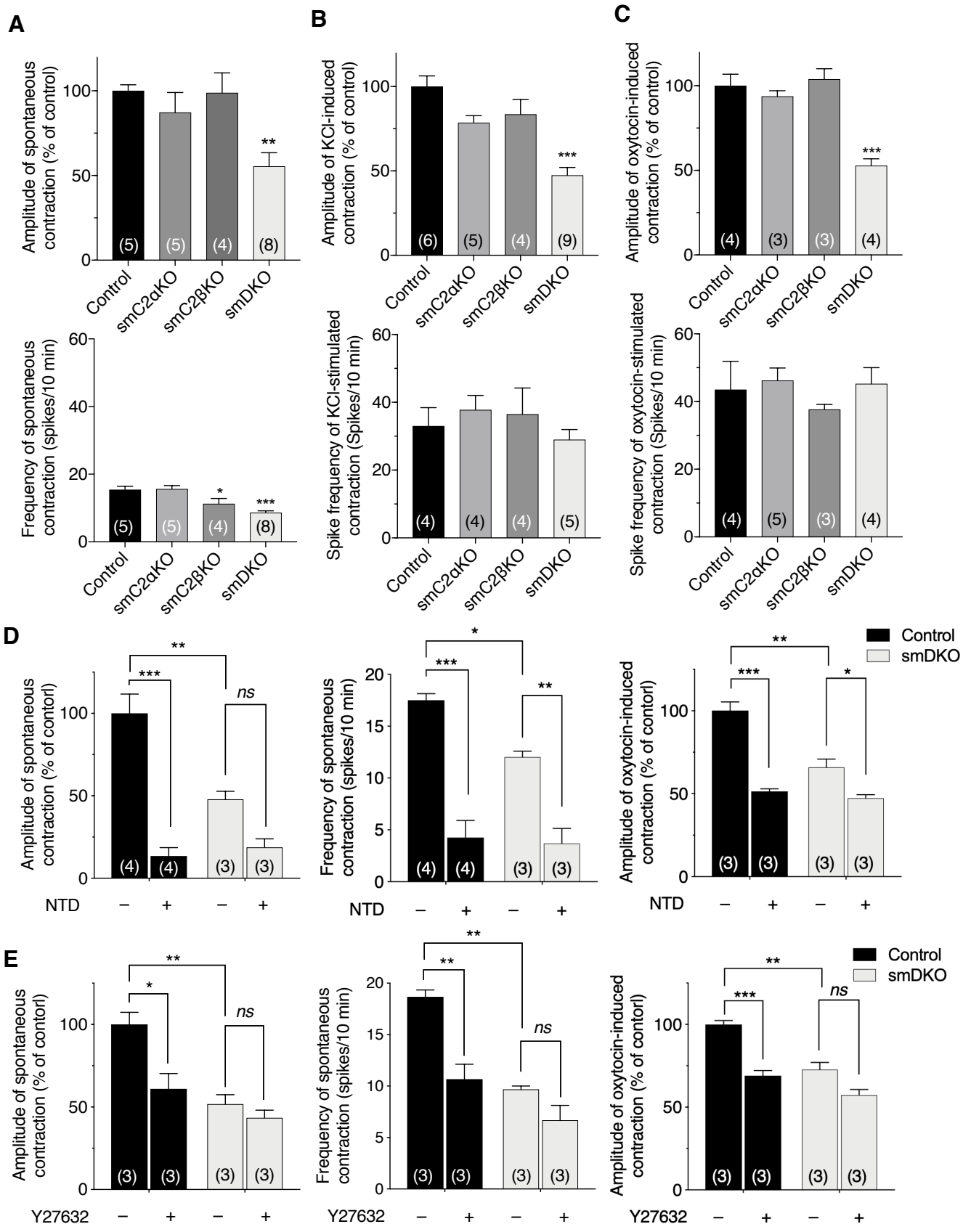


Fig. 3

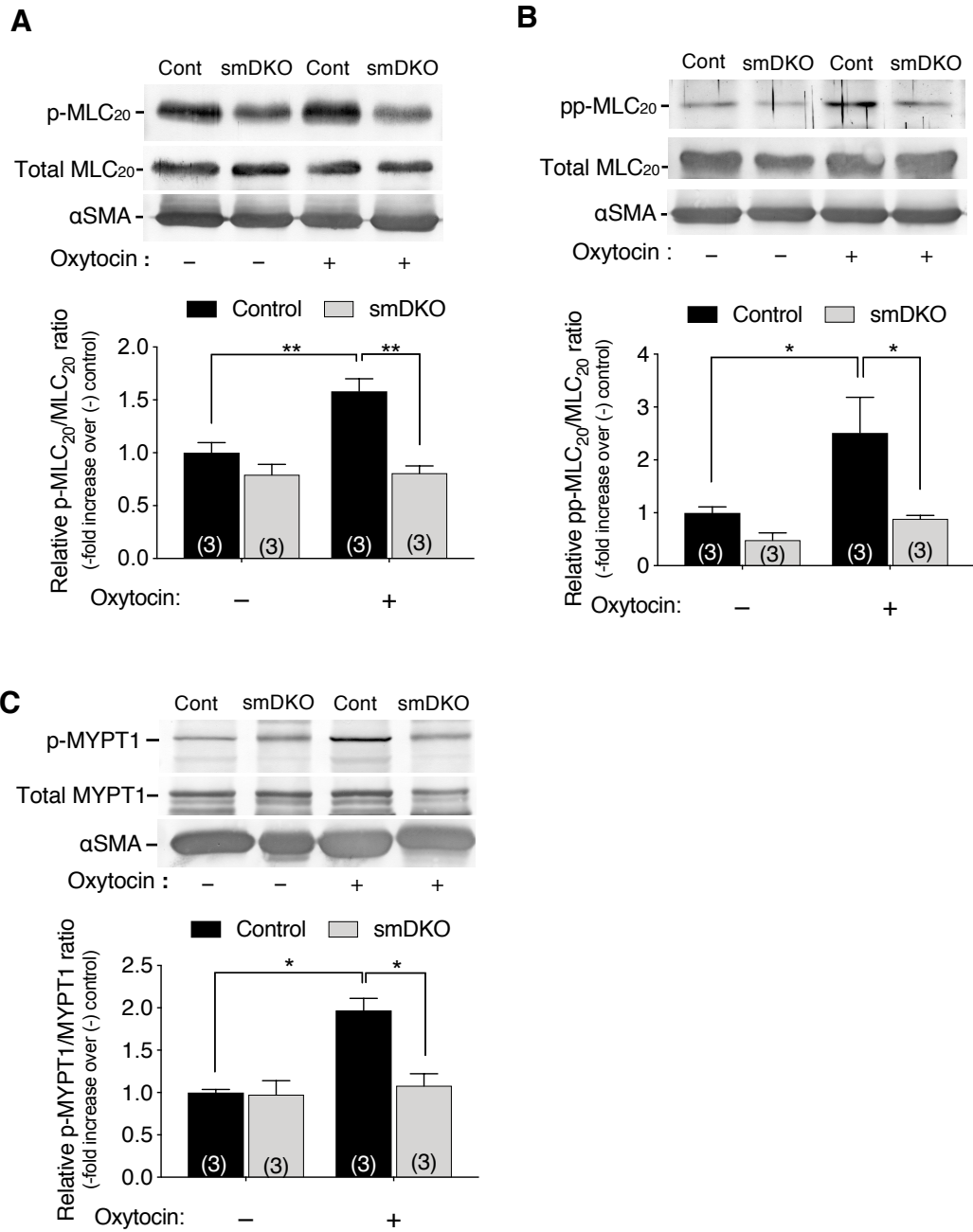


Fig. 4

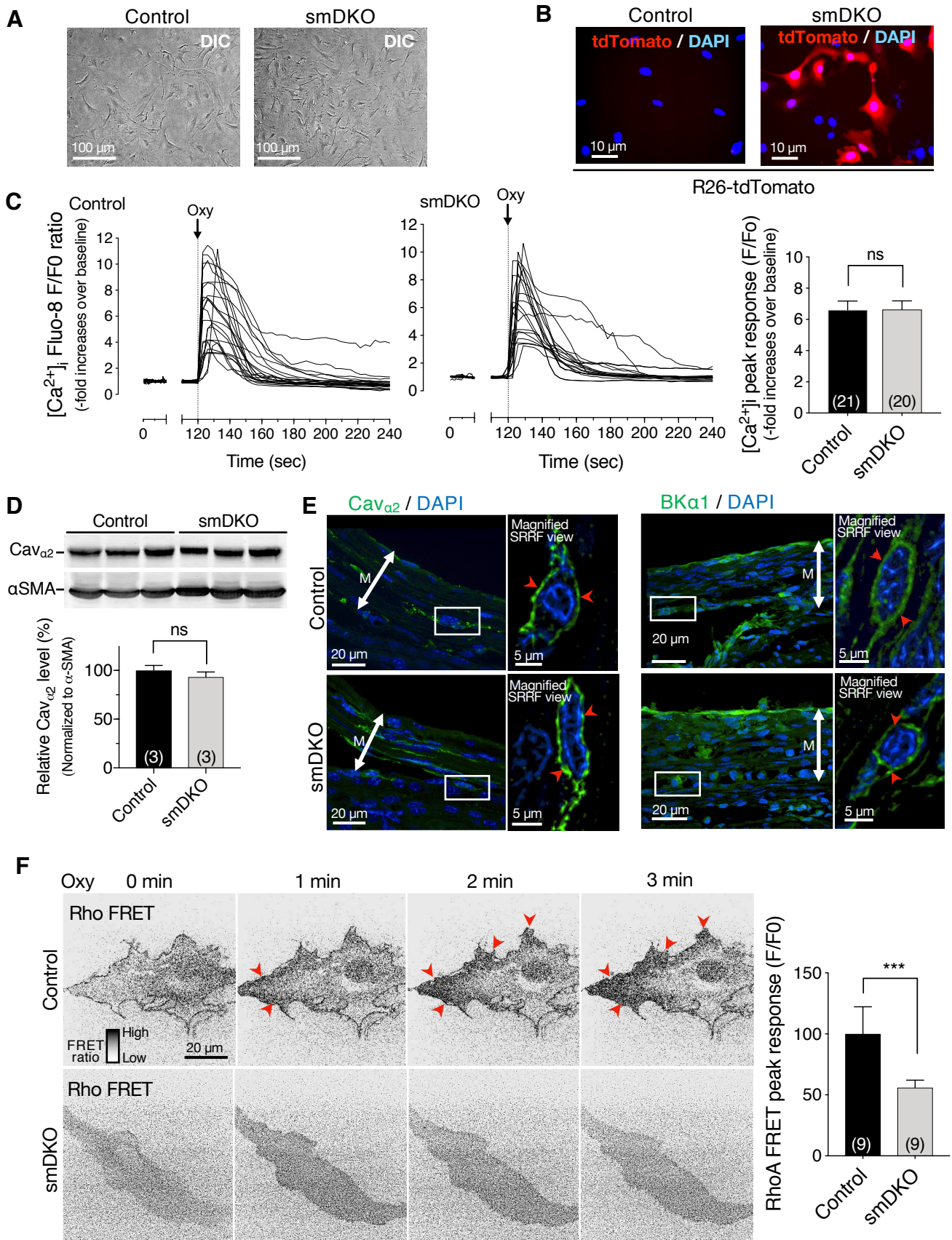


Fig. 5